AD-A083 859 ARMY MILITARY PERSONNEL CENTER ALEXANDRIA VA F/G 7/4
MICROSTRUCTURAL CHANGES IN NEUTRON AND ION IRRADIATED SILICON C--ETC(U)
APR 80 S D HARRISON

UNCLASSIFIED NL

1 OF 1
AD A
083859

END
DATE
FILMED
6-80
DTIC

LEVEL II

(1) B.S.

(6) MICROSTRUCTURAL CHANGES IN NEUTRON AND ION IRRADIATED SILICON CARBIDE

(10) Cpt. Steven D. Harrison
HQDA, MILPERCEN (DAPC-OPP-E)
200 Stovall Street
Alexandria, VA 22332

(9) Final Report, 28 Apr[redacted]80

(11)

(12) 51

Approved for public release; distribution unlimited

A thesis submitted to Rensselaer Polytechnic Institute in partial fulfillment of the requirements for the degree of Master of Science.

SECURITY CLASSIFICATION OF THIS PAGE (When Data Entered) UNCLASSIFIED

REPORT DOCUMENTATION PAGE		READ INSTRUCTIONS BEFORE COMPLETING FORM
1. REPORT NUMBER	2. GOVT ACCESSION NO. AD-A083 859	3. RECIPIENT'S CATALOG NUMBER
4. TITLE (and Subtitle) Microstructural Changes in Neutron and Ion Irradiated Silicon Carbide		5. TYPE OF REPORT & PERIOD COVERED Final Report 28 April 1980
		6. PERFORMING ORG. REPORT NUMBER
7. AUTHOR(s) Steven D. Harrison, CPT, EN, U.S. ARMY		8. CONTRACT OR GRANT NUMBER(s)
9. PERFORMING ORGANIZATION NAME AND ADDRESS STUDENT, HQDA, MILPERCEN (DAPC-OPP-E), 200 Stovall St, Alexandria, VA 22332		10. PROGRAM ELEMENT, PROJECT, TASK AREA & WORK UNIT NUMBERS
11. CONTROLLING OFFICE NAME AND ADDRESS HQDA, MILPERCEN, ATTN: DAPC-OPP-E, 200 Stovall St, Alexandria, VA 22332		12. REPORT DATE 28 April 1980
		13. NUMBER OF PAGES
14. MONITORING AGENCY NAME & ADDRESS (if different from Controlling Office)		15. SECURITY CLASS. (of this report) UNCLASSIFIED
		15a. DECLASSIFICATION/DOWNGRADING SCHEDULE

16. DISTRIBUTION STATEMENT (of this Report)

Approved for public release; distribution unlimited

17. DISTRIBUTION STATEMENT (of the abstract entered in Block 20, if different from Report)

18. SUPPLEMENTARY NOTES

Master's Thesis

19. KEY WORDS (Continue on reverse side if necessary and identify by block number)

Radiation damage, Radiation effects, Silicon carbide, SiC, Transmission Electron Microscopy, TEM, Ceramics, Controlled Fusion Reactor, Nuclear Materials

20. ABSTRACT (Continue on reverse side if necessary and identify by block number)

(Attached)

DD FORM 1 JAN 73 1473 EDITION OF 1 NOV 65 IS OBSOLETE UNCLASSIFIED

SECURITY CLASSIFICATION OF THIS PAGE (When Data Entered)

MICROSTRUCTURAL CHANGES IN NEUTRON AND ION

IRRADIATED SILICON CARBIDE

by

Steven D. Harrison

A Thesis Submitted to the Graduate

Faculty of Rensselaer Polytechnic Institute

in Partial Fulfillment of the

Requirements for the Degree of

MASTER OF SCIENCE

Approved:

John C. Corelli, Thesis Adviser

Rensselaer Polytechnic Institute

Troy, New York

28 Apr. 1980

CONTENTS

LIST OF FIGURES

ACKNOWLEDGEMENTS

The author wishes to thank the Department of Physics, USMA, United States Army for funding his graduate schooling, the Electric Power Research Institute for the project funding, Dr. John C. Corelli for his encouragement and guidance throughout the project and Dr. Charles E. Lyman for his assistance in and instruction on electron microscopy.

A very special thanks to my wife, Fran, who enabled me to keep my perspective and to Ian, Daniel and Andrew, my young sons, who provided the comic relief.

ABSTRACT

Reaction bonded silicon carbide (Norton NC 430) was examined with a 100 KV JEOL 100S TEM and a 1200 KV AEI EM7 MK II HVEM for microstructural changes induced by irradiation. Three irradiation modes were used:

1. 2×10^{24} neutrons/m^2 (E>1 MeV) irradiated at 150°C; not annealed.
2. 4×10^{24} neutrons/m^2 (E>1 MeV) irradiated at 1100°C.
3. 1 and 2 dpa from 4 MeV Ar^{40} ions at <60°C; not annealed.

In mode 1, the dislocation density increased by six orders of magnitude to 10^{14} m/m^3. Dense dislocation tangles were observed adjacent to grain boundaries and voids. No radiation-induced voids and few black spot defects were observed. In mode 2, the dislocation density was 10^{13} m/m^3 but numerous unresolved black spot defects were visible. The individual black spots are Frank dislocation loops with a diameter less than 2 nm. The density of the black spots approach $5 \times 10^{20} m^{-3}$. The argon ion damaged samples showed an unexpected loss of long range order. Neutron damage simulation with heavy ions appears to be rate dependent and may not be suitable for the investigation of ceramic materials.

It can be argued that radiation damage in silicon carbide saturates when the vacancy concentration increases sufficiently to allow recombination of interstitials at sites removed from Frank interstitial dislocation tangles. This is evident microstructurally by the high density and small size of the black spots at elevated temperature and fluence. Calculations indicate that neutrons in energy transfers are the driving force in the production of dislocations in the SiC lattice.

10 to the 14 th power CUM

ABSTRACT

Reaction bonded silicon carbide (Norton NC 430) was examined with a 100 KV JEOL 100S TEM and a 1200 KV AEI EM7 MK II HVEM for microstructural changes induced by irradiation. Three irradiation modes were used:

1. 2×10^{24} neutrons/m^2 (E>1 MeV) irradiated at 150°C; not annealed.
2. 4×10^{24} neutrons/m^2 (E>1 MeV) irradiated at 1100°C.
3. 1 and 2 dpa from 4 MeV Ar^{40} ions at <60°C; not annealed.

In mode 1, the dislocation density increased by six orders of magnitude to 10^{14} m/m^3. Dense dislocation tangles were observed adjacent to grain boundaries and voids. No radiation-induced voids and few black spot defects were observed. In mode 2, the dislocation density was 10^{13} m/m^3 but numerous unresolved black spot defects were visible. The individual black spots are Frank dislocation loops with a diameter less than 2 nm. The density of the black spots approach $5 \times 10^{20} m^{-3}$. The argon ion damaged samples showed an unexpected loss of long range order. Neutron damage simulation with heavy ions appears to be rate dependent and may not be suitable for the investigation of ceramic materials.

It can be argued that radiation damage in silicon carbide saturates when the vacancy concentration increases sufficiently to allow recombination of interstitials at sites removed from Frank interstitial dislocation tangles. This is evident microstructurally by the high density and small size of the black spots at elevated temperature and fluence. Calculations indicate that neutrons in energy transfers are the driving force in the production of dislocations in the SiC lattice.

PART 1

INTRODUCTION AND BACKGROUND

Silicon Carbide (SiC) is a candidate material for use as a first wall in nuclear fusion reactors.[1] The primary disadvantage of this material is its brittle nature which is characteristic of all ceramics and the attendant wide statistical variations in its fracture strength.[1,2,3] Several studies of the mechanical properties of SiC have shown that the fracture strength for reaction bonded SiC initially decreases and then remains fairly constant with irradiation to a neutron fluence of $\sim 2\text{-}3\times10^{25} n/m^2$ E>1 MeV.[2,3,4] The reaction bonded SiC used in these studies is a three phase material consisting of α-SiC, β-SiC and free silicon produced by mixing a 600 mesh SiC grit with colloidal graphite and a polymeric binder, shaped as desired, heated to boil away the binder and then immersed in liquid silicon in a vacuum furnace. The infiltrating silicon reacts with the deposited graphite to form SiC. The resulting material has large grains (5-20μm) of α-SiC (a hexagonal close packed polytype), smaller grains (2-5μm) of β-SiC (a zinc blend structure) and a free silicon phase of from 3 to 10 weight percent.[5]

The reaction bonded SiC used by Matheny,[3] Malloy[4] and in the present study is produced by the Norton Company, Worcester, Massachusetts, and is designated as NC430.[3,4] Characterization of this unirradiated material by a transmission electron microscope (TEM) reveals that the strength of the material is a function of the boundaries between epitaxial growths on the α-SiC grains into the β-SiC phase. Below its melting temperature, the silicon phase has a glueing affect on the matrix.[5]

Previous researchers have reported extremely low dislocation densities in SiC foils examined with a TEM. The typical defects observed were stacking faults or twins.[6] The value reported for a dislocation

density is 10^6 to $10^7 m/m^3$ which is a "puzzling feature".[6] The lack of dislocations and dislocation movement is due to the brittle, strong and spatially directed bond between silicon and carbon. Any motion of a dislocation involves the breaking of these bonds and thus requires "unusual circumstances" to promote the dislocation's movement.[6] These circumstances were observed by Stevens[7] in extracted fracture chips of SiC taken from samples of reaction bonded SiC broken at 900°C and 1100°C. In each instance, dislocations were found in the β-SiC with a $\vec{b} = a_o[110]$ and a slip plane of [111]. Photomicrographs of SiC at 1100°C show a dislocation density of $\sim 10^{13}\ m/m^3$. Stevens attributes the presence of dislocations to the action of stress concentrations occurring near the crack tip of a sample being fractured.[7]

Price[8] has examined pyrolytic β-SiC irradiated with neutrons at temperatures less than 1000°C and reported on defects that appear as small dark spots that are Frank dislocation loops lying on [111] planes with a diameter of from 2 nm to 5 nm. Above 1000°C, he observed voids ranging from 5 nm to 200 nm in diameter. He comments on fragmented stacking faults but does not mention dislocations.[8]

In summary, research into SiC has shown that as a result of fracturing dislocation densities increase near the fracture surface and that with irradiation, dislocation loops and voids appear.

PART 2

EXPERIMENTAL PROCEDURE

A. Sample Preparation

A variety of irradiation modes and TEM foil preparation sequences were utilized to examine a wide range of samples and to establish the most fruitful avenue of research.

1. Irradiation modes

a. Neutron irradiation. Samples were taken from NC430 bars used in a three point fracture test.[3] Two fluences were used:

1) 2×10^{24} neutrons/m^2 (E>1 MeV); temperature of irradiation <200°C; no annealing.

2) 4×10^{24} neutrons/m^2 (E>1 MeV); temperature of irradiation = 1100°C.

b. Ion irradiation. Chips of NC430 (2.5mmX 2.5mmX 100μm) were irradiated with 3.5 MeV Argon ions ($T \lesssim 60$°C during irradiation) at the SUNY Albany facility to damages of 1 and 2 dpa (fluences of 8.4×10^{19} ions/m^2 and 1.7×10^{20} ions/m^2 respectively).

2. Foil production methods

a. Ion milling. A Commonwealth Scientific ion micro miller was used to thin to perforation ion irradiated and 2×10^{24}n/m^2 samples previously sized to 2.5mmX 2.5mmX 100μm, with a diamond saw and power lapping machine using 800 grit boron carbide abrasive. The micro-miller was the most time consuming step in sample preparation. Typically, a sample required 40 hours to thin when using both accelerating guns at 6KV;

100μA beam current and a sample tilt of 25°. The ion irradiated samples required 80 hours since only one side could be eroded.

b. Extraction replicas. Extraction replication was used quite successfully to examine $4 \times 10^{24} n/m^2$ samples and produced excellent results with considerably less effort than ion milling. However, the use of a High Voltage Electron Microscope (HVEM) is imperative since the sample thickness is ∿1.5μm. A description of the extraction replication technique can be found in ASTM 04-547000-28.

B. Microscopy Procedures

In the course of this research, two electron microscopes were used:

1. The JEOL 100S belonging to the RPI Materials Engineering Department, equipped with a double tilt goniometer stage and has an accelerating voltage of 100KV.
2. An AEI EM MKII #10 HVEM belonging to the New York State Department of Health Laboratory, Albany, N.Y., equipped with a double tilt goniometer stage and having an accelerating voltage of 1200KV was used extensively. This machine allows the researcher to view through a six fold increase in sample thickness to 1.5μm. On both machines, exposures were made on Kodak 4463 film.

Throughout the study, care was taken to use standard and accepted electron microscopy procedures. Especially significant was the effort to obtain dynamical two beam conditions to allow quantitative analysis of the photomicrographs.

PART 3

RESULTS

The results of this study are the images and diffraction patterns taken on the electron microscope of the samples prepared from irradiated material. What this study accomplished will be presented as a series of photographs with a brief explanation describing the irradiation parameters, method of sample preparation, microscope used for examination, general and specific features in the image and comments on the diffraction pattern when pertinent. Brief discussions of the literature and some detailed conclusions will be inserted for clarity, as required.

A. Unirradiated NC430

Unirradiated NC430 was examined and the photographs are presented to provide a contrast to the irradiated material. This sample was ion milled to perforation and examined with the JEOL 100S TEM.

<u>Figure 3.1</u>

1. <u>Figure 3.1.a.</u> The granular structure of a reaction bonded SiC is apparent. The large grain marked with an A is α-SiC. The grain at B is β-SiC. Immediately below the B is a dislocation in contrast. The .2μm pore in the center of the photograph at C is a result of the manufacturing process. It lies immediately next to a truncated portion of a grain and across a linear disordered structure similar to an epitiaxial growth interface described by Sawyer.[6]

2. Figure 3.1.b. A line of faceted pores delineated by crystal planes is apparent at A. Through B, an interface with smaller pores is observed.

Figure 3.1   Unirradiated NC430

a) Typical Microstructure of NC430

b) Grain Boudaries Containing Faceted Voids

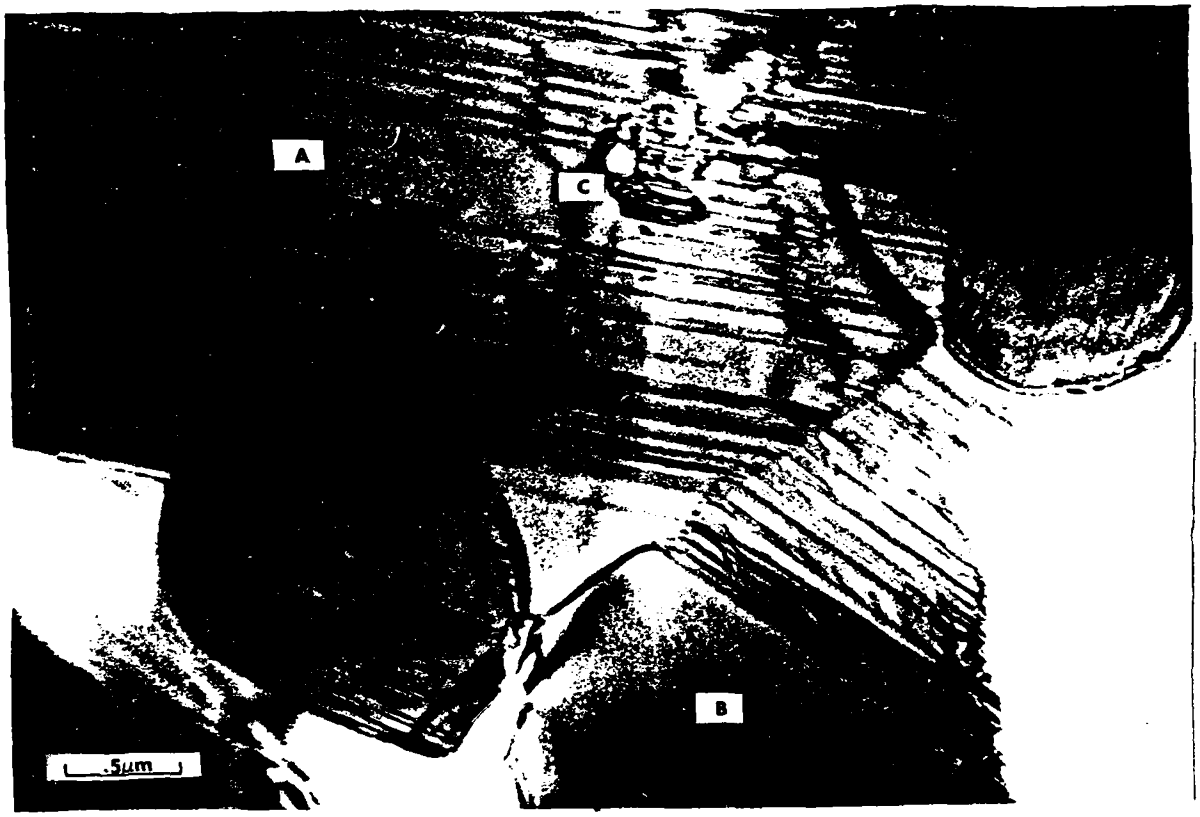

a)

b)

B. Neutron Irradiated ($2 \times 10^{24} m^{-2}$)

Figures 3.2 through 3.5 are of NC430 irradiated to $2 \times 10^{24} n/m^2$ (E>1 MeV) at 150°C and not annealed. Samples were thinned on the ion mill and examined with the JEOL 100S TEM.

Figure 3.2

1. Figure 3.2.a. Dislocations tangles are startlingly apparent in this picture of a α-SiC grain. The dislocation density in the center of the grain is $1.5 \times 10^{13} m/m^3$ and increases to $1 \times 10^{14} m/m^3$ at the outer edge where the grain boundary stops the dislocation movement. (See Appendix for dislocation density calculation). One outstanding feature is the L shaped dislocation line at A on the figure.

2. Figure 3.2.b. Same area as in Figure 3.2.a but viewed from the other side of the sample. The dislocation dissociation at A may indicate the presence of an impurity or some additional crystal defect. The L shaped dominant feature in each photomicrograph can be explained as the interaction of two dislocations having intersecting slip planes.[9] Similar features can be seen in the areas containing tangled dislocations.

3. Figure 3.2.c. This diffraction pattern shows that the reflection being used in this experiment is a $[1\bar{2}10]$ type and the material is α-SiC (6H polytype) with a beam direction of [0001].

Figure 3.2 2 x $10^{24} n/m^2$ Dislocation on Grain Boundary

a) Dislocation Tangles Adjacent to Grain Boundary, View 1.

b) Dislocation Tangles and L Shaped Dislocation.

c) Diffraction Pattern

a)

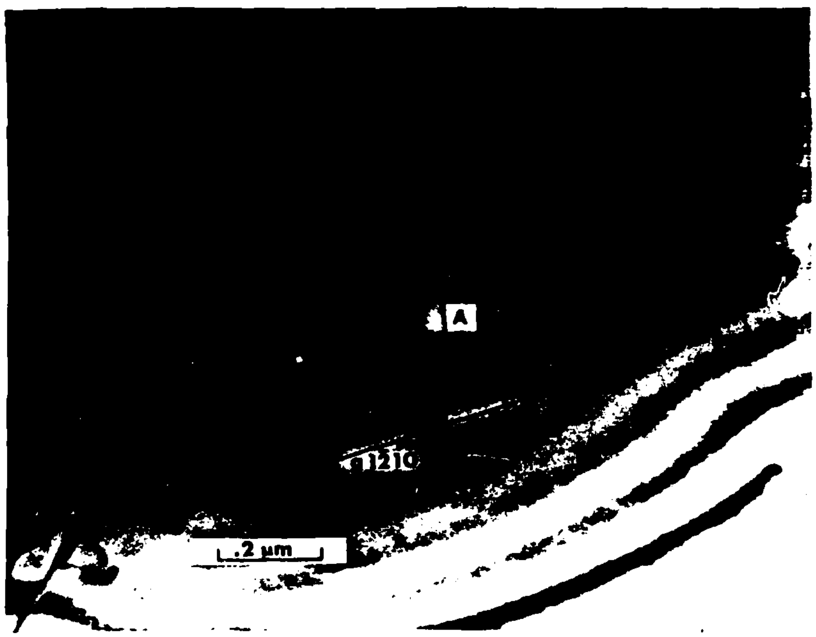

b)

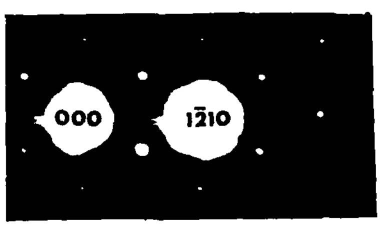

c)

Figure 3.3

1. Figure 3.3.a. A gradient in dislocation density is again apparent with the grain boundary at A and the inclusion or void at B causing a pile up of dislocations and a tangled appearance. The dislocation density near A is approximately 10^{15} m/m^3. The L shaped dislocation interaction again appears to be the dominant recognizable feature. At C, the apparent pinning of a dislocation as it moves through the crystal is evident.

2. Figure 3.3.b. Same area as Figure 3.3.a enlarged, showing dissociating dislocation on one leg of an L shaped dislocation interaction.

Figure 3.3 $2 \times 10^{24} n/m^2$ Dislocations Blocked by Void

a) Dislocations Surrounding Void and Along Grain Boundary

b) Dislocations Interactions

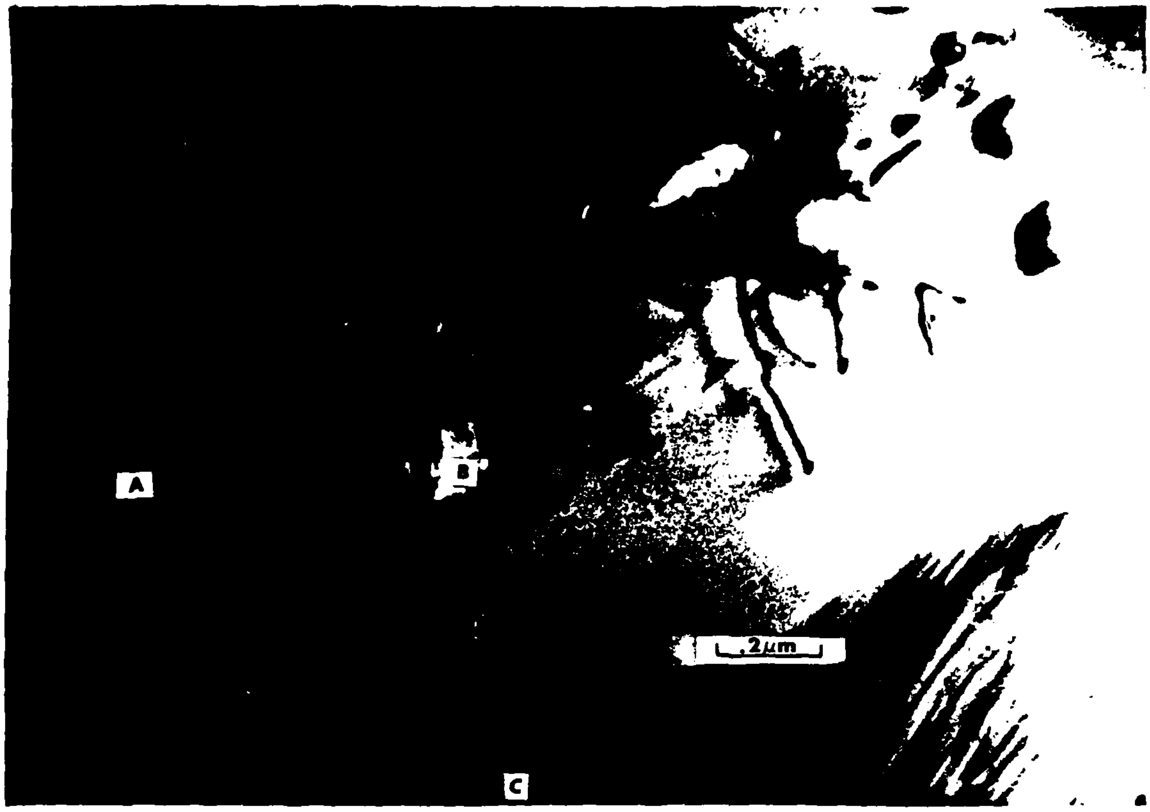

a)

b)

<u>Figure 3.4</u>

<u>1. Figure 3.4.a.</u> In this picture, two L shaped dislocations are being formed at A as described in Read.[9] At B, the dislocation is interacting with the stacking faults while at C, the dislocations are not interacting with the stacking faults.

<u>2. Figure 3.4.b.</u> The numerous dislocations in this picture show the characteristic L shaped dislocation interaction and sub boundary array (A) associated with a void.

Figure 3.4 2 x 10^{24}n/m^2 Dislocation Interactions

a) Dislocation Intersections

b) Dislocations Near Void

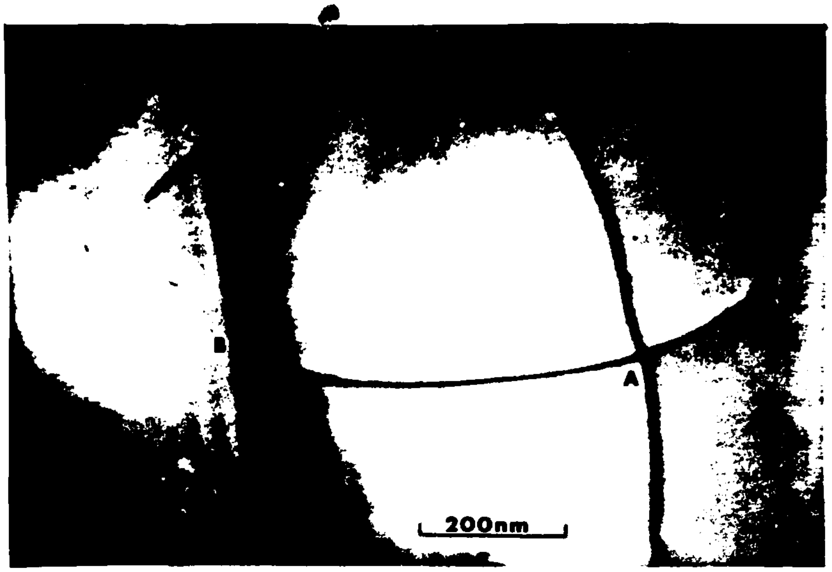

a)

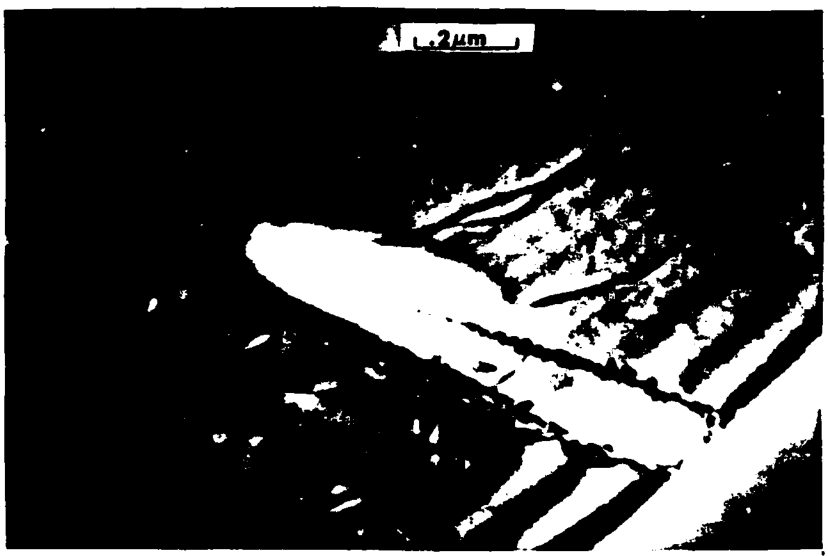

b)

Figure 3.5

1. Figure 3.5.a Dislocation networks appear at node A and B with an L shaped dislocation at C.

2. Figure 3.5.b. A different diffraction vector reveals that small circular spots are apparent at the thin outer edge of the area. The spot at A shows the black and white lobe described by Price[8] and is a classical black spot defect with a diameter of $\sim$20nm. Crossing the diffraction vectors $\{[1\bar{2}10] \times [3\bar{3}00]\}$ yields the slip plane for the dislocations as [0001] which is the h.c.p. equivalent of the [111] plane in the simple cubic described in the literature.[7]

Figure 3.5 2 x 10^{24}n/m^2 Different Reflections of Some Dislocation Network

a) [$1\bar{2}10$] Reflection

b) [$3\bar{3}00$] Reflection

a)

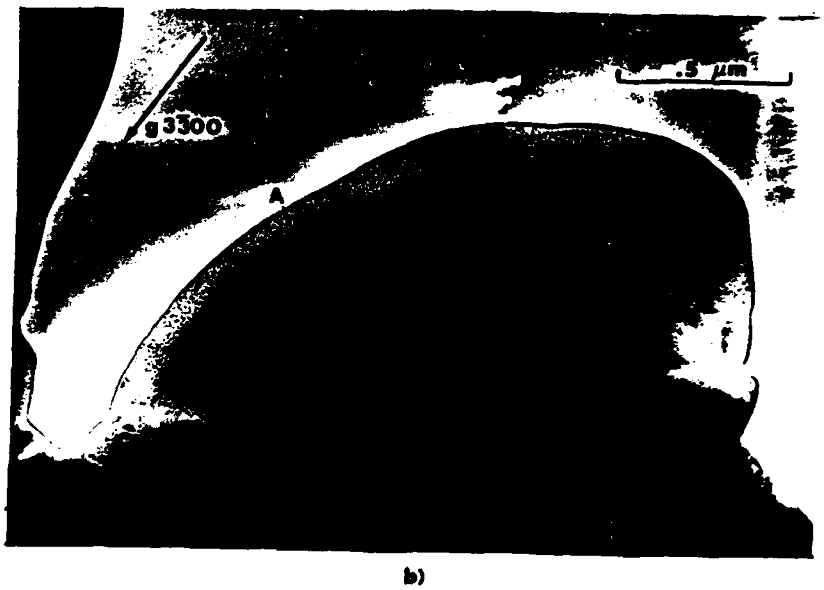

b)

C. Neutron Irradiated ($4 \times 10^{24} n/m^{-2}$)

Figures 3.6 through 3.8 are of NC430 irradiated to 4×10^{24} neutrons/m^2 E>1 MeV at 1100°C. Samples were extracted from fracture surfaces and examined on the HVEM.

Figure 3.6

1. Figure 3.6.a. This picture shows dislocations and black spots on a fracture chip containing two grains of β-SiC (see Figure 3.6.c). At A, the dislocation pile up at the grain boundary is consistent with other observations. The dark area in the center is the result of the extremely wedged shape of the sample and the corresponding thickness (approximately 1.8μm) in the middle. The black spots are evident throughout the foil with a density of $5 \times 10^{20} m^{-3}$, but are most obvious at B.

2. Figure 3.6.b. Dislocations and linear arrays of black spot defects are apparent in the entire picture. The dislocations appear to be independent of the black spots.

3. Figure 3.6.c. This diffraction pattern of the area in Figure 3.6.b shows a β-SiC pattern with a beam direction of [110] and a fine structure in the {111} spots. This splitting is the result of two grains overlaying each other in this relatively thick sample or twinning. A problem with using the HVEM is the difficulty in getting dynamical two beam conditions. In this case, the 220 family of spots is excited approximating the dynamical conditions used earlier.

Figure 3.6 $4 \times 10^{24} n/m^2$ Fracture Chip Showing Dislocations and Black Spots

a) Chip Containing Two β-SiC Grains

b) Portion of β-SiC Grain

c) Diffraction Pattern of 3.6.b.

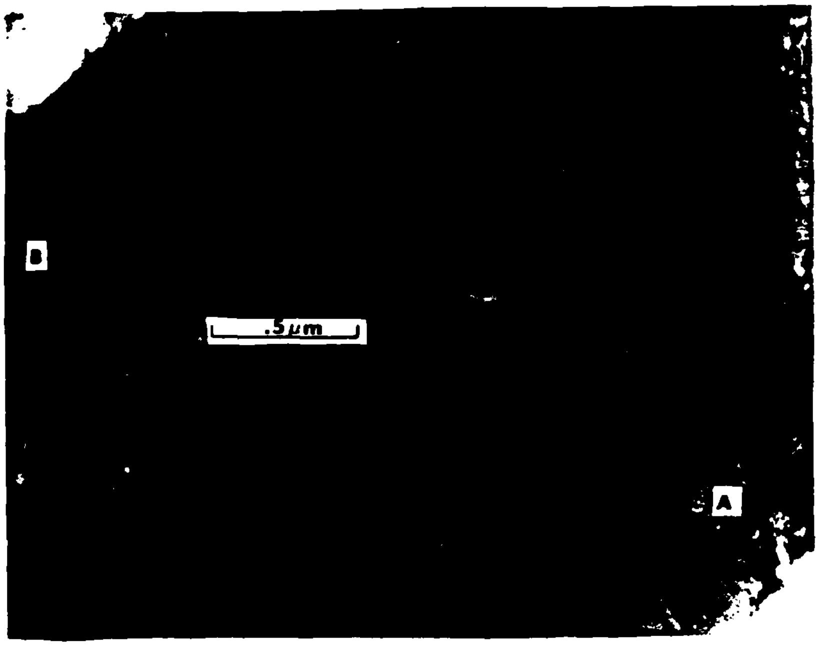

a)

b)

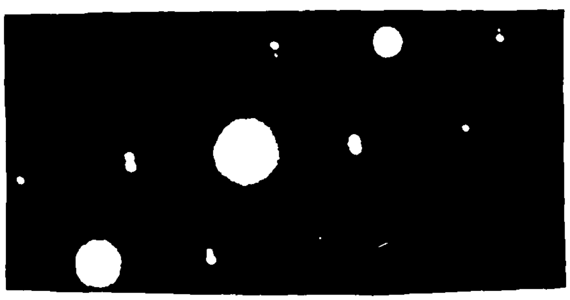

c)

Figure 3.7

Figures 3.7.a, 3.7.b, 3.7.c. These photomicrographs show the black spots and dislocation quite clearly. The average size of black spot is 2nm and the density is $4 \times 10^{20} m^{-3}$. The dislocation density is variable but is approximately $10^{13} m/m^{3}$. It was difficult to estimate the thickness of these fracture chip samples.

Figure 3.7 Dislocation Interaction and Black Spot Defects $4 \times 10^{24} n/m^2$

a) Fracture Chip Showing Dislocations and Black Spot Defects

b) Dislocation Interactions

c) Black Spot Defects

a)

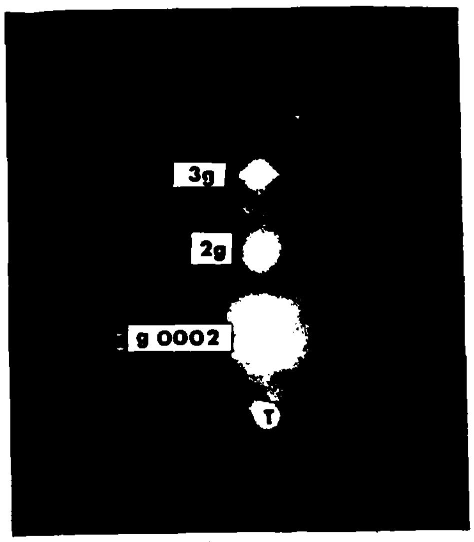

b)

Figure 3.8

1. Figure 3.8.a. This weak beam dark field (g/3g) photomicrograph was taken by Dr. C. E. Lyman. The technique highlights the defects in the material by exciting a diffracted beam far removed from the central transmitted beam causing a reversal in contrast, thereby increasing the resolution. The black spots and dislocations are quite obvious.

2. Figure 3.8.b. This diffraction pattern shows the conditions at which the image 3.8.a, was taken.

Figure 3.8 Weak Beam Dark Field of Fracture Chip
($4 \times 10^{24} n/m^2$)

a) Weak Beam Dark Field of Fracture Chip Containing Defects.

b) Diffraction Pattern of Figure 3.8.a.

D. Heavy Ion Irradiated

Figure 3.9

This sample of NC430 was irradiated with 3.5 MeV Ar+ ions to 8.4×10^{19} ions/m^2 (∿1dpa) at a temperature <60°C, ion milled and examined with the JEOL 100S.

1. Figure 3.9.a. The most startling aspect of this picture is the lack of the typical NC430 structure. Even though several grains are in the field of view, the characteristic stacking faults and wide variation of diffraction conditions between grains is not apparent.

2. Figure 3.9.b. This diffraction pattern $\vec{B}$=[0001] shows that the basic 6H pattern is overlaid with a concentric ring pattern characteristic of a material composed of extremely small grains (less than 10nm) randomly oriented. This combination of ring and spot pattern is typical of an electrodeposited material upon a like material base.(10)

The argon ions appear to have destroyed a portion of the α-SiC resulting in large volume where the long range order of the crystal is non-existent. This observation is consistent with the statement made by Dr. J. W. Choyke that ion bombardment would leave SiC essentially amorphous.(11)

Figure 3.9 Argon Irradiated (1dpa)

a) Typical Microstructure of Ion Irradiated Sample

b) Diffraction Pattern of Edge in Figure 3.9.a.

a)

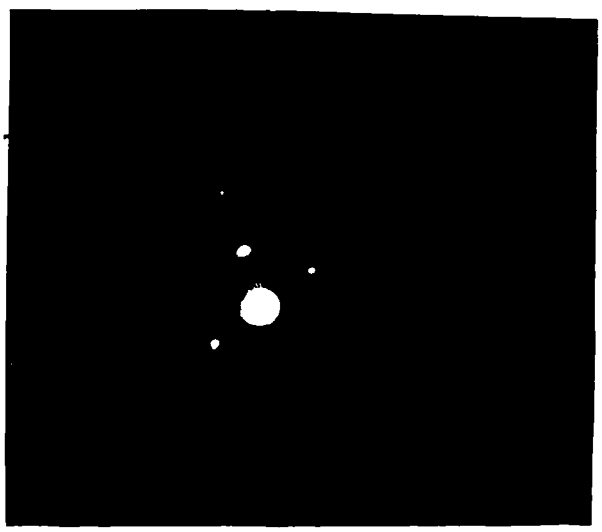

b)

Figure 3.10

This sample was irradiated to 1.7×10^{20} ions/m^2 (2dpa) with 3.5 MeV Ar+ ions at $\sim$<60°C and milled to perforation. Examination was conducted with the HVEM.

1. Figure 3.10.a. As with the 1 dpa sample, the long range order of the α-SiC has essentially been destroyed and small grains of SiC overlay the larger α-SiC.

2. Figure 3.10.b. The diffraction pattern has a spot and ring pattern showing that a portion of the crystal has lost its order in the selected area. The spot pattern corresponds to the $[01\bar{1}0]$ α-SiC beam direction and the ring patterns are 0002 and $2\bar{1}12$, confirming the 6H α-polytype and showing that in this sample α-SiC recrystallized on the α-SiC grain.

Figure 3.10 Argon Irradiated (2dpa)

a) Typical Ion Irradiated Microstructure

b) Diffraction Pattern of Figure 3.10.a.

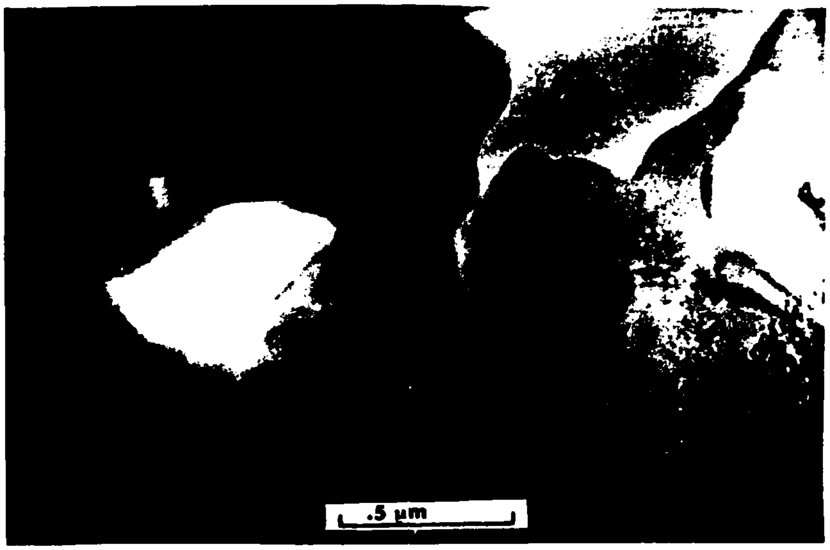

a)

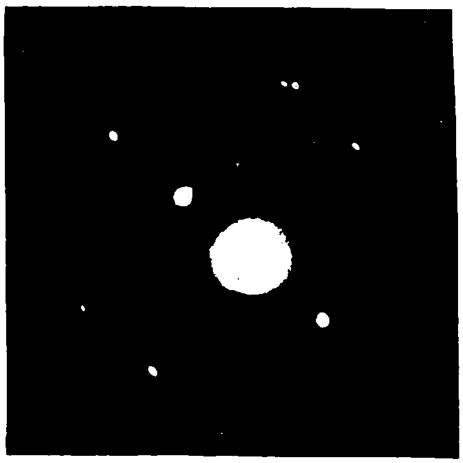

b)

PART 4

DISCUSSION AND CONCLUSIONS

A. DISCUSSION

Neutron Irradiation

The complex nature of reaction bonded SiC results in variations in the reported properties of the material following irradiation.[2,3,4] The most significant variable, other than displacements per atom, appears to be the temperature history. If irradiated at a low (∿200°C) temperature and not annealed, there appears to be a 10-15% decrease in fracture strength. On the other hand, material that has been exposed to 1200°C retains much of its fracture strength. In this study, similiarities and differences were noted in the microstructural changes of SiC following irradiation in high and low temperature.

The SiC irradiated at 200°C to $2 \times 10^{24} n/m^2$ and not annealed has pronounced dislocation tangles but an extremely low density of black spot defects (Figures 3.2, 3.3, 3.4, 3.5). At lower temperatures, the isolated vacancies created by knock-ons act as recombination sites for interstitials and upon reaching a high enough concentration due to an increased fluence, compete with dislocation loops as sinks for interstitials.[12] In this sample, the concentration of vacancies for recombination appears to be insufficient to slow the growth of the Frank loops initially produced by collapsing cascades. The bonding of SiC is extremely strong (having a displacement threshold of 106 eV compared to 30-40 eV for most metals) and spatially directed so the mobility of interstitials is significantly greater than vacancies. From the results it can be argued that the interstitials migrate predominantly to the Frank loops, which act as sinks and grow out of the black spot size. These dislocation loops interact and form the tangles observed in Figure 3.2.a.

The energy associated with these tangles is computed in the appendix and is ten orders of magnitude less than the amount of energy deposited in the SiC by the neutrons. It is, therefore, completely possible for this mechanism to be neutron induced.

The L shaped dislocations observed in SiC were predicted by Read,[9] as the result of two dislocations having the same Burgers vector but orthogonal slip planes intersecting. The presence of the dislocation tangles and pile ups can adversely affect the fracture strength as demonstrated by Olander[13] when the stress concentration induced by the pile up causes a microcrack longer than the Griffith's criteria crack (70μm).[3] The initial decrease in fracture strength observed by Matthews[2] can be explained by this mechanism.

At higher temperatures and fluences, the concentration of vacancies quickly reaches a level where they deny, via recombination, interstitials for loop growth. In the $4 \times 10^{24} n/m^2$ irradiated at 1100°C, this phenomena is manifested by the numerous black spots ($5 \times 10^{20} m^{-3}$) which are static Frank loops. The rapid decrease in interstitials causes the saturation of macroscopic damage parameters noted by Malloy.[4] It is significant that this saturation shoulder in the damage profile occurs at a temperature of 1100°C, above the present design temperature range (600°C-900°C) of a fusion reactor. Figures 3.9 and 3.10 show the intimate nature of the black spot defects and the larger dislocation loops indicating that some transition may be taking place to the temperature regime where the damage does not saturate.[12]

Ion Irradiation

One of the most successful techniques used to simulate high dpa in metals has been the use of heavy ion bombardment to produce the knock-ons along with preinjection or co-injection of He to simulate the void forming

properties of fusion spectrum. In this study, the SiC irradiated with 3.5 MeV Ar^{40} ions to damage levels above that observed in the neutron irradiation did not behave as a metal would. The diffraction pattern of an α-SiC grain is overlaid with a ring pattern characteristic of β-SiC but having a grain size much less than the 5-10μm grain contributing to the primary diffraction spot pattern. From the image and the diffraction pattern one concludes that the ion beam has introduced so much damage so quickly that the material lost all order beyond a few unit cells distance at the irradiation temperature of 60°C. The rate of the damage introduction appears to be significantly greater than the mobility of the interstitial and vacancy species in the matrix. The collapsing cascades and cascade overlap has completely destroyed the grain. The interstitials residing in the matrix would have their structure altering properties "washed out" by the effect of the heavy ions.

B. CONCLUSIONS

From the evidence of the photomicrographs and application of radiation damage theory and experiment, it can be concluded from the microstructure of reaction bonded SiC that the damage introduced by neutrons will saturate quickly at fluences of $\sim 10^{24} n/m^3$ and temperatures of $\sim 1100°C$. At higher fluences, this saturation effect should be observed at increased temperatures before a catastrophic growth of defects takes place. Reaction bonded Norton SiC NC-430 appears to be an excellent candidate for high temperature, high fluence environments by virtue of the defect saturation.

Further study of radiation damage in SiC needs to be done using neutron sources as opposed to heavy ion sources since the material is sensitive to the rate at which damage is introduced. A high damage rate completely destroys the long range order of the grains which is in striking contrast to the microstructural changes observed due to neutron irradiation, at the same dpa level.

LITERATURE CITED

1. L. H. Rovner, G. H. Hopkins, Nucl. Tech. 29 (1976).

2. R. B. Matthews, J. Am Ceram. Soc. 57 (1974).

3. R. A. Matheny, J. C. Corelli and G. G. Trantina, J. Nucl. Mat. 83 (1979).

4. J. Malloy, Personal conversations, Rensselaer Polytechnic Institute (1979-1980).

5. G. R. Sawyer, T. F. Page, J. Mat. Sci. 13 (1978).

6. R. Stevens, J. Mat. Sci. 7 (1972).

7. R. Stevens, J. Mat. Sci. 6 (1971)

8. R. J. Price, J. Nucl. Mat. 48 (1973).

9. W. T. Read, Jr., Dislocations in Crystals, McGraw-Hill Book Co., Inc. 1953.

10. J. W. Eddington, Practical Electron Microscopy, Van Nostrand Reinhold Co., New York, 1976.

11. J. M. Choyke, private conversation Westinghouse Electric Corporation (Sept. 1979).

12. L. W. Hobbs, J. Am. Ceram. Soc. 62 (1979).

13. D. R. Olander, Fundamental Aspects of Nuclear Fuel Elements, TlD-26711-P1 ERDA, 1976.

APPENDIX

The elastic energy associated with dislocations may be computed and when multiplied by the dislocation density gives an estimate of the volumetric energy introduced into the crystal structure. A comparison with the amount of energy the neutrons can deposit will show that it is energetically possible to create the dislocations with the neutron fluence of these experiments.

<u>A. Energy deposited by neutrons</u>. Assuming that all the neutrons have an energy of 1 MeV, the energy fluence for the sample in Figure 3.2 is 2×10^{24} MeV/m^2. The intensity of the transmitted beam, $\Phi(X) = \Phi_o \exp[-\Sigma_T X]$, with Φ_o the incident energy fluence while the absorbed portion is $\Phi_o - \Phi(X)$. Therefore,

$$\Phi_A = \Phi_o - \Phi(X) = \Phi[1-\exp(-\Sigma_T X)]$$

$$X = .25 \text{ cm}$$

$$\Sigma_T = \rho \frac{N_A}{M} (\nu_{Si}\, \sigma_{si} + \nu_C \nu_C)$$

$$\rho = 3.21 \text{ gm/cm}^3$$

$$N_A = \text{Avagadro's number} = .6025 \times 10^{24}$$

$$M = \text{Molecular weight} = 40$$

$$\nu_{Si} = \nu_C \equiv \text{atom fraction/molecule} = 1$$

$$\sigma_{Si} \equiv \text{total cross section for Si @ 1 MeV} = 5.6 \text{ barns}$$

$$\sigma_C \equiv \text{total cross section for C @ 1 MeV} = 2.66 \text{ barns}$$

$$\Sigma_T = .366 \text{ cm}^{-1}$$

$$\Phi_A = 2 \times 10^{24} [1 - \exp(-.366 \times .25)] \text{ MeV/m}^2$$

$$= 1.75 \times 10^{23} \text{ MeV/m}^2$$

Since the thickness in which this energy is deposited is 2.5×10^{-3}m, the energy density deposited in the sample is 7×10^{25} MeV/m^3 or 4.4×10^{12}J/m^3.

B. Energy of a dislocation. The commonly accepted method for calculating the energy of a dislocation is outlined by Olander.[13] The approximations are:

$$E_{e\ell} = \frac{Gb^2}{4\pi} \ln \left(\frac{r_1}{r_0}\right) \approx Gb^2 \qquad \text{for a screw dislocation}$$

$$E_{e\ell} = \frac{Gb^2}{4\pi(1-\nu)} \ln \left(\frac{r_1}{r_0}\right) \approx \frac{Gb^2}{1-\nu} \qquad \text{for an edge dislocation}$$

Given that:

Shear modulus $\equiv G = 1.958 \times 10^{10}$ neutons $m/^2$for SiC

Poisson's ration $\equiv \nu = 0.173$

Lattice parameter $\equiv a_o = 3.8 \times 10^{-10}$m

Burger's vector $\equiv b = \frac{a_o}{2} [110]$; $b^2 = \frac{a_o^{\ 2}}{4} [1^2 + 1^2 + 0] = 9.5\text{x}10^{-20} m^2$

r_1 = distance to grain boundary

r_0 = core of dislocation $\sim 15 \times 10^{-10}$m

The energies are:

$E_{e\ell}$(screw) = 1.86×10^{-9} J/m = 1.16 MeV/m of dislocation

$E_{e\ell}$(edge) = 2.25×10^{-9} J/m = 1.4 MeV/m

C. Dislocation density. The density of dislocations in a material is the length of dislocations per unit volume. Determining the volume is dependent upon accurately determining the thickness of the specimen in the region where the measurement is made. One procedure is to use the extinction fringes (see Figure 3.2.b).[10] The extinction distance ξ_g is:

$$\xi_g = \frac{\pi V_c \cos\theta}{\lambda F_g} \quad \text{with (hkil) = } (1\bar{2}10)$$

Volume of unit-cell $\equiv V_c = (3.073)^2(15.08) = 142.4$ Å^3

Probe electron wavelength $\equiv \lambda = .037$ Å

Bragg angle $\equiv \theta = \sin^{-1} \left(\frac{\lambda}{2d}\right) = \sin^{-1} \left(\frac{.037\text{Å}}{2(1.54)\text{Å}}\right) = .0123$ radians

Structure factor $\equiv F_g = \sum_{i}^{N} f_i(\theta)\exp\,[2\pi i(hk\ell)\cdot(u_i v_i w_i)]$

Atomic scattering factor $\equiv f_c(\theta) = .83$ Å From Edington with $\frac{\sin\theta}{\lambda} = .325$
(for carbon)

Atomic scattering factor $\equiv f_{Si}(\theta) = 1.385$ Å
(for silicon)

Space cell information from Wyckoff

Carbon atom positions $(u_i v_i w_i)$

000; 001/2; $\frac{1}{3}\,\frac{2}{3}\,\frac{1}{6}$; $\frac{1}{3}\,\frac{2}{3}\,\frac{5}{6}$; $\frac{2}{3}\,\frac{1}{3}\,\frac{2}{3}$; $\frac{2}{3}\,\frac{1}{3}\,\frac{4}{3}$

Silicon atoms positions: $(u_i v_i w_i)$

001/8; 005/8; $\frac{1}{3}\,\frac{2}{3}\,\frac{1}{8}$; $\frac{1}{3}\,\frac{2}{3}\,\frac{7}{24}$; $\frac{2}{3}\,\frac{1}{3}\,\frac{23}{24}$; $\frac{2}{3}\,\frac{1}{3}\,\frac{35}{24}$

Substituting $u_i v_i w_i$ for all twelve atoms and reducing for $(hk\ell) = (1\bar{2}0)$. $F_g = 6\,[f_c(\theta) + f_{si}(\theta)] = 13.29$ Å

$$\text{Therefore } \xi_g = \frac{\pi(142.4 \text{ Å}^3)\cos(0.0123 \text{ rad})}{(.037 \text{ Å})(13.29 \text{ Å})} = 910 \text{ Å}$$

$\frac{1}{2}\,\xi_g = 455$ Å $\frac{7}{2}\,\xi_g = 3185$ Å

$\frac{3}{2}\,\xi_g = 1365$ Å $\frac{9}{2}\,\xi_g = 4095$ Å

$\frac{5}{2}\,\xi_g = 2275$ Å $\frac{11}{2}\,\xi_g = 5005$ Å

For example, the thickness of a sample between the third and fourth extinction fringes varies from 2275 Å to 3185 Å in a roughly linear fashion.

Using the above as an estimate of the thickness an area of dislocations is mapped out and the length of dislocations is measured. The ratio is converted to m/m^3 and a dislocation density is computed. In Figure 3.2.a, the dislocation density varied from $1.5 \times 10^{13}\ m/m^3$ to $1 \times 10^{14} m/m^3$.

D. The Energy of Dislocation Tangles. Taking the results from B and C above the volumetric energy density ranges from ($1.5 \times 10^{13} m/m^3$) x 1.16 MeV/m) or 1.74×10^{13} MeV/m^3 for the low density area assuming screw dislocations to 1.4×10^{14} MeV/m^3 assuming edge dislocation in the dislocation pile-up area. Alternately, if one assumes that atoms are separated by 3 Å, a meter of dislocations represents 3×10^{19} atoms displaced or 3.18×10^5 MeV/m at a threshold displacement energy of 106 eV. At the dislocation density in question, the energy varies from 4.8×10^{18} MeV/m^3 to 3×10^{19} MeV/m^3.

E. Comparison between energies. From the above calculations the energies are:

1) Energy deposited by neutrons $\approx 7 \times 10^{25}$ MeV/m^3

2) Energy associated with dislocation tangles is estimated from 1.7×10^{13} MeV/m^3 to 3×10^{19} MeV/m^3.

Comparing these figures it appears that the neutron energy fluence exceeds the energy in the dislocation tangles by 6 to 12 orders of magnitude.